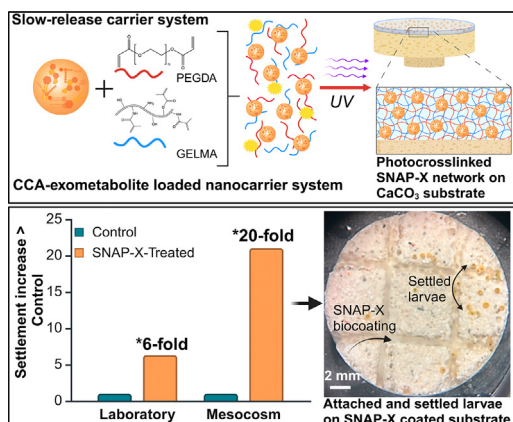


Research Article

Biomimetic chemical microhabitats enhance coral settlement



A hybrid biomaterial, SNAP-X, was engineered to mimic natural chemical landscapes, enhancing coral settlement by over 20-fold. By sustained cue release, this technology addresses recruitment failure on degraded reefs and has broader applications in marine ecology and biomaterials science.

Samapti Kundu, Simone Potenti, Zachary A. Quinlan, Helena Willard, Justin Chen, Timothy Noritake, Natalie Levy, Zahra Karimi, Hendrikje Jorissen, Joshua R. Hancock, Crawford Drury, Linda Wegley Kelly, Luisa De Cola, Shaochen ChenR3D consortiumDaniel Wangpraseurt

dwangpraseurt@ucsd.edu
(D. Wangpraseurt).

Highlights

Coral settlement drives reef growth and biodiversity, but remains a major bottleneck in reef restoration.

We engineered SNAP-X, a hybrid biomaterial that releases settlement cues via a nanoparticle–biopolymer delivery system.

SNAP-X enhances coral settlement over 20-fold, advancing reef restoration with translational potential in chemotaxis and nanomedicine research.

Trends in Biotechnology, Month 2025,
Vol. xx, No. xx
<https://doi.org/10.1016/j.tibtech.2025.03.019>

Research Article

Biomimetic chemical microhabitats enhance coral settlement

Samapti Kundu^{1,2}, Simone Potenti³, Zachary A. Quinlan^{1,4}, Helena Willard⁵, Justin Chen², Timothy Noritake², Natalie Levy^{1,2}, Zahra Karimi², Hendrikje Jorissen⁴, Joshua R. Hancock⁴, Crawford Drury⁴, Linda Wegley Kelly¹, Luisa De Cola^{3,6}, Shaochen Chen², R3D consortium and Daniel Wangpraseurt^{1,2,*}

Anthropogenic stressors pose substantial threats to the existence of coral reefs. Achieving successful coral recruitment stands as a bottleneck in reef restoration and hybrid reef engineering efforts. Here, we enhance coral settlement through the development of biomimetic microhabitats that replicate the chemical landscape of healthy reefs. We engineered a soft biomaterial, SNAP-X, comprising silica nanoparticles (NPs), biopolymers, and algal exometabolites, to enrich reef microhabitats with bioactive molecules from crustose coralline algae (CCA). Coral settlement was enhanced over 20-fold using SNAP-X-coated substrates compared with uncoated controls. SNAP-X is designed to release chemical signals slowly (>1 month) under natural seawater conditions, and can be rapidly applied to natural reef substrates via photopolymerization, facilitating the light-assisted 3D printing of microengineered habitats. We anticipate that these biomimetic chemical microhabitats will be widely used to augment coral settlement on degraded reefs and to support ecosystem processes on hybrid reefs.

Introduction

Coral reefs are one of the most biodiverse and economically important ecosystems globally, providing a home to more species per unit area than any other marine ecosystem [1]. The economic significance of coral reefs is vast, particularly for the 13% of the global population residing within 100 km of these ecosystems [2]. They contribute an estimated US\$375 billion annually to global economies through coastal protection, aquaculture, tourism, fisheries, as well as pharmaceuticals [3]. Over the past five decades, coral reefs have faced significant anthropogenic pressures, primarily stemming from climate change [4] and urbanization [5]. Estimates suggest that, by 2050, 70–90% of coral reefs will be severely degraded [2]. The survival and resilience of coral reefs depend greatly upon the successful recruitment of various benthic invertebrate larvae, such as corals, sponges, and mollusks, which help build the complex structure of the reef habitat and contribute to the maintenance of reef biodiversity [6].

Similar to most sessile marine invertebrates, corals exhibit a planktonic larval phase, facilitating broad dispersal to locate an optimal habitat for settlement [7]. Large-scale hydrodynamics influence the initial dispersal of coral larvae across the open water [8]. However, once flow velocity attenuates in proximity to the benthos, larvae can actively discern and select their specific microhabitats using distinct chemical cues [9,10]. This selective process aids the identification of suitable substrates for attachment, ultimately influencing postsettlement mortality rates and subsequent reef growth dynamics [11]. On healthy coral reefs, CCA have a pivotal role in inducing

Technology readiness

SNAP-X, a biomimetic material designed to enhance coral settlement by replicating the chemical landscape of coralline algae on healthy reefs, has reached Technology Readiness Level (TRL) 4. It has been successfully tested in both laboratory and mesocosm environments, demonstrating up to a 20-fold increase in coral settlement compared with controls, and sustained bioactive cue release for over 1 month. To progress to higher TRLs, key challenges include optimizing cost-effective large-scale production of exometabolites and demonstrating effectiveness across diverse reef environments globally. Achieving these milestones will pave the way for the integration of SNAP-X into global coral restoration and reef engineering initiatives.

¹ Scripps Institution of Oceanography, University of California San Diego, San Diego, USA

² Aiyso Yufeng Li Family Department of Chemical and Nano Engineering, University of California San Diego, San Diego, CA, USA

³ Department of Pharmaceutical Sciences, University of Milan, Milan, Italy

⁴ Hawai'i Institute of Marine Biology, University of Hawai'i, Kāne'ohe, USA

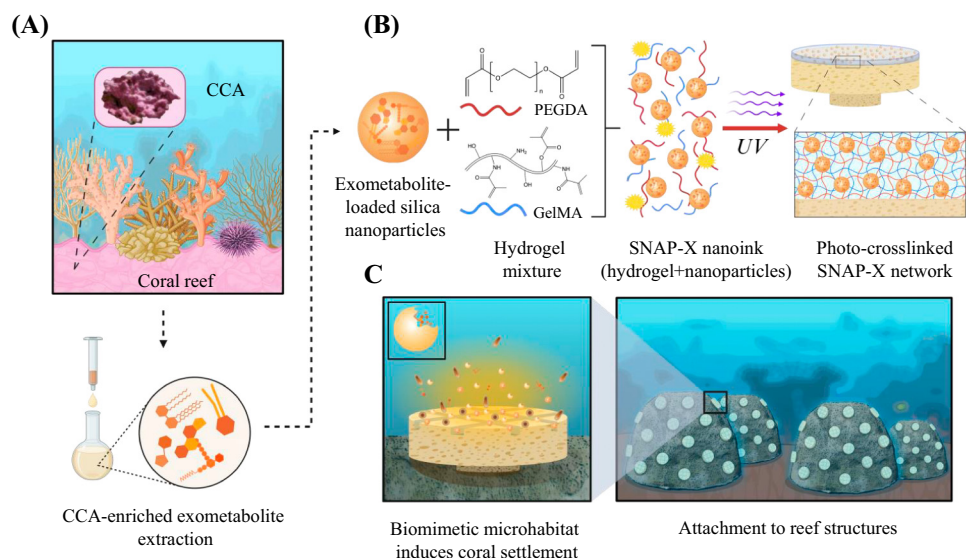
⁵ Computational Science Lab, University of Amsterdam, Netherlands

⁶ Department of Molecular Biochemistry and Pharmacology, Istituto di Ricerche Farmacologiche Mario Negri, IRCCS, 20156 Milano, Italy

*Correspondence:
dwangpraseurt@ucsd.edu
(D. Wangpraseurt).

coral larval settlement and metamorphosis [10,12–17]. Recent advances in metabolomics and cheminformatics identified the distinct chemical landscape of CCA [18,19]. CCA metabolites exuded into the surrounding water (so-called ‘exometabolites’) induce settlement of coral larvae even in the absence of CCA [18]. By contrast, competitive macro- and turf algae release other chemical signals [19] that can inhibit settlement [20]. As coral reefs shift toward more fleshy algal-dominated systems, the chemical landscape of coral reefs changes [19], which contributes to recruitment failure and ultimately describes a major bottleneck for the restoration and rehabilitation of coral reefs worldwide [21–23].

The threats facing coral reefs have overwhelmed many conservation efforts, and are now calling for more active, transformative interventions, including human-assisted evolution [24] and microbiome and probiotic therapy [25]. Recently, it was suggested that adjacent engineering fields offer promising solutions via the development of functional nanomaterials or advanced 3D biofabrication approaches to accelerate ecosystem engineering processes [26–30]. We propose that coral restoration and rehabilitation can greatly benefit from integrating advances in bioengineering and nanotechnology [31]. These disciplines, traditionally focused on biomedical applications and human tissue engineering, have seen substantial progress in the engineering of functional drug carrier systems [32], living materials [33,34], and biohybrid materials [35,36]. Here, we use a biomimetics approach to engineer SNAP-X, a biocompatible nanoink comprising silica NPs and exometabolites derived from CCA [10,14,18,37–39], which are embedded within a hydrogel matrix (Figure 1A,B). SNAP-X can be rapidly applied to reef substrates via photopolymerization, facilitating the light-assisted 3D printing of chemical microhabitats (Figure 1C). Our results show that such biomimetic microenvironments promote coral settlement, suggesting their application to accelerate reef restoration and hybrid reef engineering by mimicking natural chemical landscapes.



Trends in Biotechnology

Figure 1. Schematic of the recruitment-enhancing SNAP-X coating for coral restoration and hybrid reef engineering. (A) Solid-phase extraction of crustose coralline algae (CCA; *Hydrolithon* sp.)-enriched exometabolites. (B) CCA exometabolites were encapsulated in silica nanoparticles and combined with a hydrogel mixture comprising gelatin methacrylate (GelMA) and poly(ethylene glycol) diacrylate (PEGDA). The resulting nanoink was crosslinked on CaCO_3 -based coral restoration substrates via photopolymerization. (C) The SNAP-X coating gradually enriches the chemical landscape responsible for coral settlement and can be locally attached to larger reef restoration frameworks.

Results

CCA exometabolite-loaded silica NPs

The molecular composition of CCA exometabolites was characterized using liquid chromatography tandem-mass spectrometry (LC-MS/MS) [40], revealing a major contribution of lipids and lipid-like molecules as well as organic acids and derivatives to the pool of molecular ion features (Figure 2A and Figure S1 in the supplemental information online). These features were classified into chemical classes, including carboxylic acid derivatives, carbohydrates and conjugates, amino acids, steroids, fatty amides, and ethers (Figure 2A,B and Figure S1 and Text S1 in the supplemental information online).

Comparative thermogravimetric analysis (TGA) (Figure 3A) and Fourier transform infrared (FTIR) spectroscopy (Figure S2 in the supplemental information online) confirmed the successful encapsulation of exometabolites. TGA measured a mass loss of 29% at 350–550°C for exometabolite-loaded silica NPs compared with a mass loss of 12% at 110°C for empty NPs (Figure 3A) [41]. While the mass loss of empty NPs was primarily attributed to the desorption of water molecules from the silica surface, the additional mass loss at higher temperatures for exometabolite-loaded silica NPs originated from the thermal decomposition of organic compounds [41,42]. The mean hydrodynamic diameter of the empty and exometabolite-loaded silica NPs was 67 nm and 42 nm, respectively (Figure 3B). The difference in size resulted from the presence of complex metabolites that can modulate the supramolecular chemistry involved in the formation of nanosilica [43] (Figure S3 in the supplemental information online).

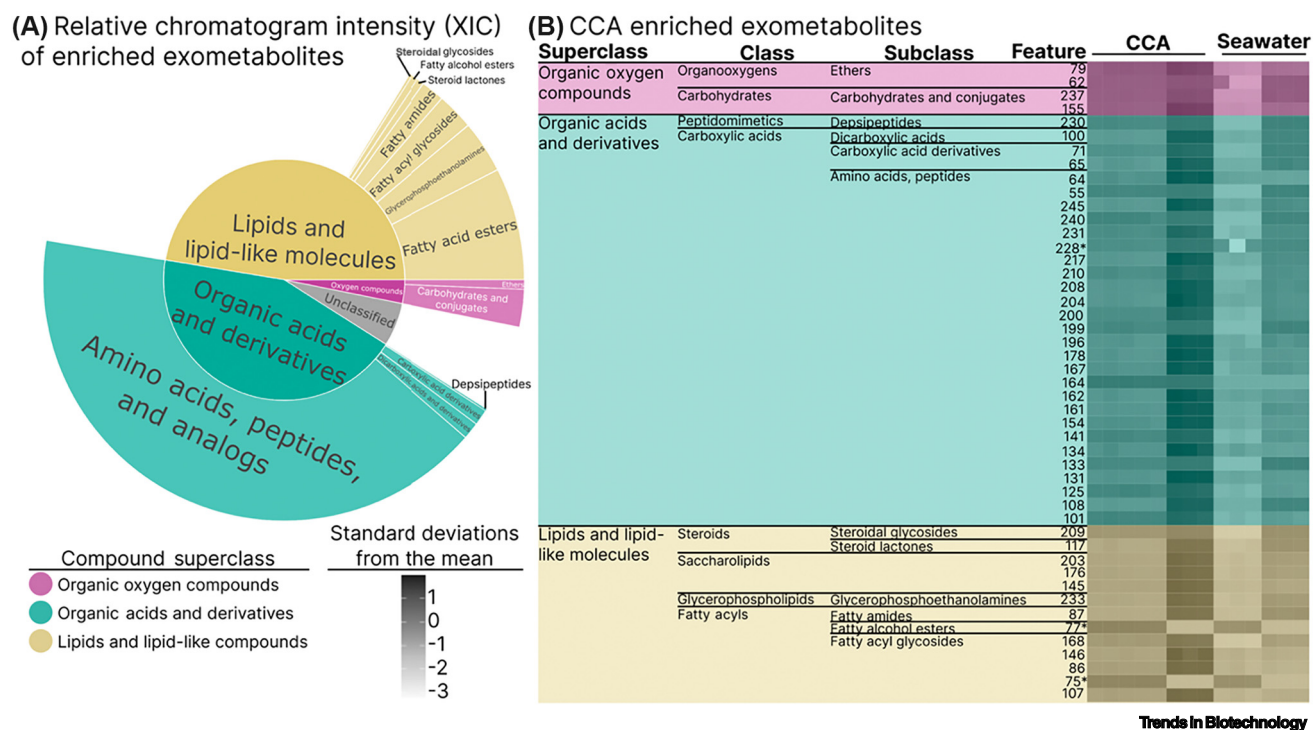


Figure 2. Chemoinformatics of crustose coralline algae (CCA) exometabolites. (A) Sunburst plot. Inner pie wedges and outer wedges represent the relative extracted ion chromatogram (XIC) intensity of each superclass and subclass, respectively. Unclassified subclasses were not included as outer wedges. (B) Heatmap of classified ion features of CCA-enriched exometabolite pools for two independent sampling time points (March and June). The cells of the heatmap are colored as relative chromatogram enrichment (XIC) across each sample, calculated as standard deviations from the mean (z-scored). Ion features not classified at any level were not included (see Figure S1B in the supplemental information online for a full heatmap). Ion features and pie wedges are colored by broad chemical classification (Superclass). Note: '*' represents the metabolites present during a single timepoint only.

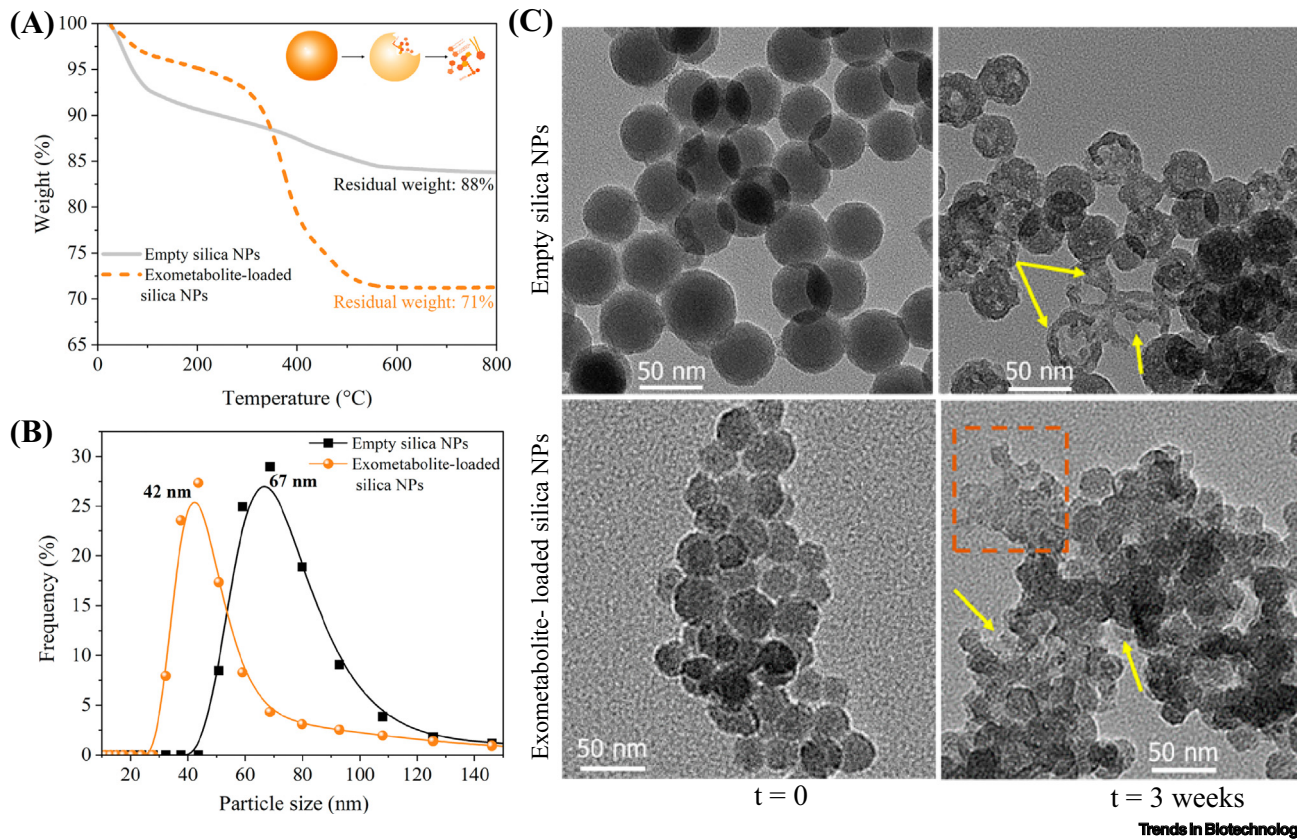


Figure 3. Material characterization of exometabolite-loaded silica nanoparticles (NPs). (A) Organic mass loss (% weight) was determined through thermogravimetric analysis (TGA) for empty and exometabolite-loaded silica NPs. (B) Particle size distribution of empty silica NPs versus exometabolite-loaded silica NPs assessed using dynamic light scattering. (C) Transmission electron microscopy (TEM) image of empty silica NPs and exometabolite-loaded silica NPs after synthesis (t = 0) and after 3 weeks in seawater (t = 3 weeks). Breakdown of the NPs is highlighted (orange broken line) and is characterized by the loss of NP sphericity (yellow arrows) and the presence of agglomeration.

Hydrogel composition

To modulate the degradation properties of the hydrogel matrix, we used a combination of two biopolymers for photopolymerization: poly(ethylene glycol) diacrylate (PEGDA) and gelatin methacrylate (GelMA). We optimized the final concentration (w/v %) of the hydrogel mixture for their enhanced stability in natural seawater conditions over extended periods (>3 months; Figure S4 in the supplemental information online), while maintaining high porosity (>30%; Figure S5 in the supplemental information online) to enable diffusion of gases and chemical signals through the hydrogel network (Figures 1B and 4A). The hydrogel was photo-crosslinked on top of CaCO_3 as a thin layer (500–600 μm) containing uniformly dispersed NPs (Figure 4B).

Release kinetics of SNAP-X

Release kinetics were assessed using a common model molecule (cytochrome C [44]) and revealed up to fourfold slower release rates for the developed NP-hydrogel system (~20% mean release after 28 days) compared with the standalone NPs (~89% mean release after 28 days; Figure 4A and Figures S6 and 7 in the supplemental information online). Mathematical modeling showed that the measured rates were well predicted based on silica hydrolysis in a stabilized environment (i.e., hydrogel [45]; Text S2 and Figure S6 in the supplemental information online). To mimic water motion, we also performed release tests under constant shaking, which revealed

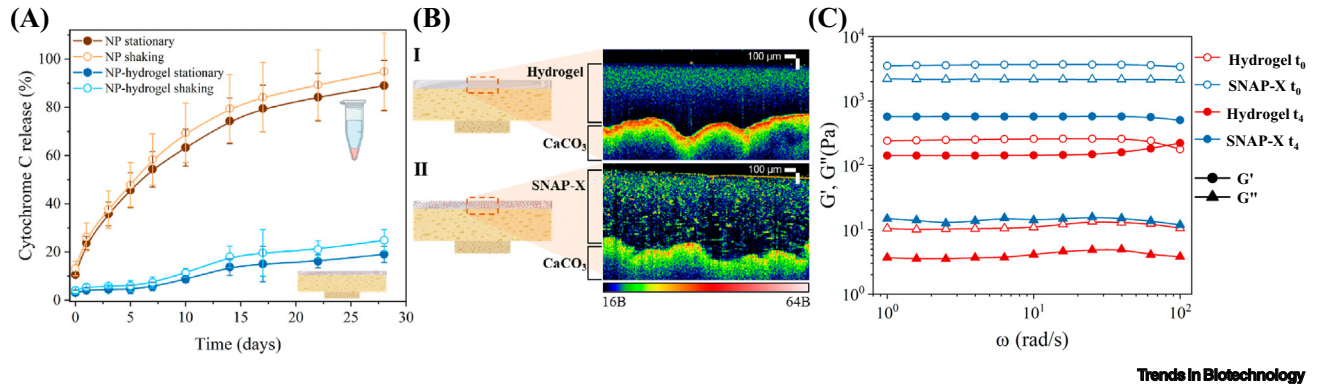


Figure 4. Material properties of SNAP-X nanoink. (A) Release kinetics assessed via absorbance of cytochrome C. Data are means (\pm SE, $n = 6$). (B) Noninvasive structural imaging of (i) empty hydrogels ($525 \pm 64 \mu\text{m}$) versus (ii) cytochrome C-loaded hydrogels ($604 \pm 41 \mu\text{m}$) performed via optical coherence tomography. (C) Rheological properties of empty hydrogels and nanoparticle (NP)-loaded hydrogels. Variation of the storage modulus (G') and loss modulus (G'') of gelatin methacrylate (GelMA)-poly(ethylene glycol) diacrylate (PEGDA) hydrogel controls and SNAP-X as a function of frequency. Abbreviation: SE, standard error.

similar release rates between stationary and shaking conditions for the NP-hydrogel system [maximum difference at day 22: mean stationary, $16.10\% \pm 2.72$ standard deviation (SD); mean shaking, $21.06\% \pm 3.56$ SD, ANOVA, $F_{(1,8)} = 0.17$, $P = 0.69$; Figure 4A].

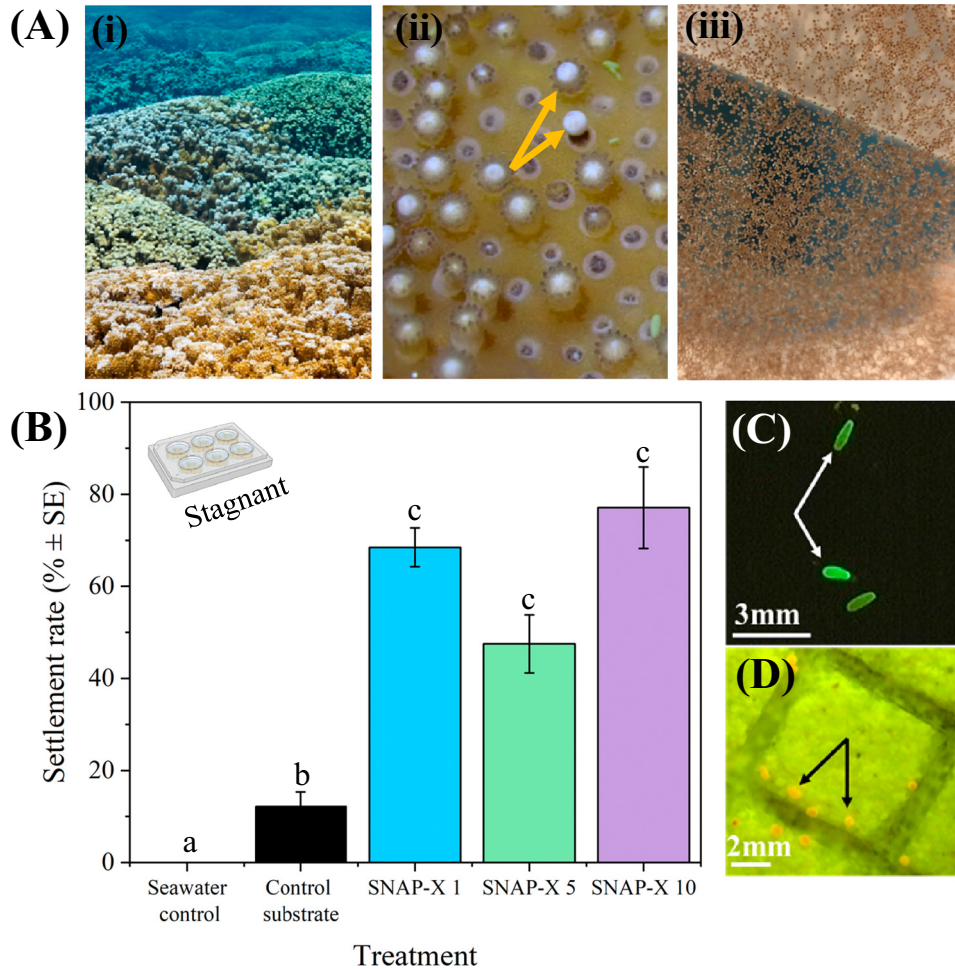
Rheological properties of SNAP-X

We evaluated the rheological properties of SNAP-X and control hydrogels over time, specifically examining changes in mechanical stability under natural seawater conditions. SNAP-X exhibited a significantly higher initial storage modulus (G') of ~ 3500 Pa ($0-70$ rad/s) compared with the control hydrogel ($G' \sim 250$ Pa, $0-70$ rad/s), highlighting the enhanced mechanical strength conferred by the incorporation of silica NPs (Figure 4C). The NPs contributed to a denser crosslinked network, improving the stability of the hydrogel in saline environments [46–49]. Over 4 weeks, the storage modulus (G') of SNAP-X gradually decreased to ~ 500 Pa ($0-70$ rad/s), while that of the control hydrogel declined to ~ 150 Pa ($0-70$ rad/s). This sustained mechanical performance of SNAP-X can be attributed to the reinforcing effect of the silica NPs, which helped maintain the elasticity of the hydrogel even in saline conditions [50,51]. This material behavior, characterized by initial stability and gradual softening, could be advantageous for coral larvae, because the firm substrate supports settlement, while the subsequent softening may promote their growth and integration into the material.

Performance of SNAP-X in coral settlement

To test the efficacy of SNAP-X in settlement assays, we first performed laboratory experiments with *Montipora capitata*, a primary reef-building coral in Hawai'i (Figure 5A). Compared with CaCO_3 -based control substrates, larvae exposed to SNAP-X exhibited up to sixfold higher settlement rates (ANOVA, $F_{(4,42)} = 40.77$, $P < 0.001$; Figure 5B). Visual observations suggested that larvae preferred to settle near the SNAP-X-coated crevices (Figure 5D and Figure S8 in the supplemental information online), suggesting the successful molecular enrichment of the substrate microhabitat. By contrast, for CaCO_3 -based control substrates, settlement rates were close to 10%, while seawater controls showed no settlement (Figure 5C).

We performed an outdoor mesocosm settlement experiment using natural seawater and continuous water flow to evaluate SNAP-X under *in situ*-like conditions (Figure 6 and Figure S9 in the supplemental information online). Settlement was enhanced by up to 20-fold using SNAP-X compared with the uncoated control substrate (ANOVA, $F_{(3,67)} = 7.09$, $P < 0.001$; Figure 6A). Under



Trends in Biotechnology

Figure 5. Laboratory settlement assays of *Montipora capitata* with SNAP-X-coated substrates. (A) *M. capitata* colonies on a reef in Hawai'i (i). Gametes (ii, yellow arrow) were collected during annual spawning and fertilized in the laboratory and reared to competency (iii). (B) Settlement rate [% ± standard error (SE)] of larvae after overnight incubation with seawater alone, uncoated control substrates (CaCO₃ coral plug), and different loading densities of SNAP-X ($n = 6$; ANOVA, statistical significance is indicated by letters; Tukey's HSD post-hoc comparisons, $P < 0.001$). (C) Example image of swimming larvae in the seawater control with characteristic elongated shape (white arrows). (D) Example image of attached and settled larvae (black arrows) on SNAP-X-coated substrates.

continuous water flow, we also detected a significant effect of the concentration of CCA exometabolites on settlement induction (Figure 5A), which was not present in our laboratory experiments (compared with Figure 5). Substrates coated with SNAP-X 10 (i.e., tenfold enhanced exometabolite loading concentration) showed settlement densities that were up to 170% higher compared with the medium loading concentration (SNAP-X 1; Figure 6A). In turn, for SNAP-X 0.1 (i.e., tenfold reduced loading concentration), there was no significant difference in settlement compared with uncoated control substrates (ANOVA, $P = 0.59$, Figure 6A).

Diffusion modelling of chemical cues

3D chemical diffusion modeling showed that the concentration of a hypothetical chemical cue (with an average molecular weight of 12 kDa; Text S2) was enhanced toward the surface of the

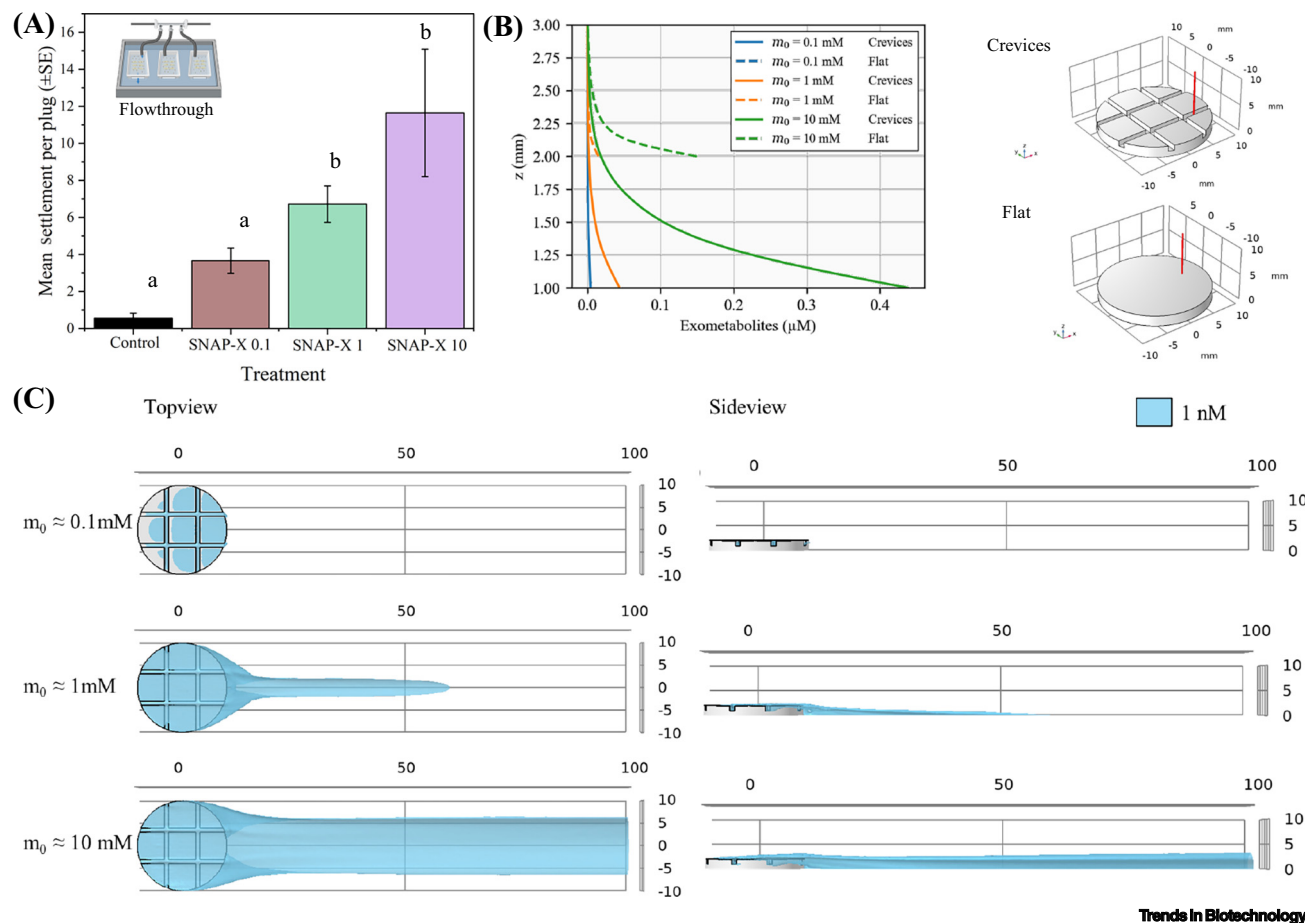


Figure 6. Mesocosm experiments and 3D diffusion modeling of a biomimetic chemical microhabitat under natural water flow. (A) Settlement rates of *Montipora capitata* in a natural mesocosm flowthrough system ($n = 6$; ANOVA, significance values are denoted by different letters; Tukey's HSD post-hoc comparisons, $P < 0.01$). (B,C) 3D chemical diffusion modeling of the distribution of a hypothetical chemical cue at an incident flow velocity of 1 cm s^{-1} . (B) Distribution of chemical cues toward the surface of SNAP-X-coated biomimetic substrates with varying loading concentrations and microtopographies (flat and crevices). (C) Spatial distribution of the halo of chemical cues for varying loading concentrations of SNAP-X-coated biomimetic substrates. Abbreviation: SE, standard error.

substrate (Figure 6B). The developed SNAP-X coating created a halo of settlement-inducing metabolites that extended well beyond the coating ($>10 \text{ cm}$; Figure 6C). Such chemical landscape enrichment was dependent on the initial loading density of exometabolites (Figure 6C), as well as fluid flow and mass transfer properties (Figure S10 in the supplemental information online).

Discussion

Biomimetic chemical microhabitats attract coral larvae

To enhance coral settlement in their natural environment, it is crucial that chemical signals are released from the biomaterial slowly over time, ideally over a timeframe of several weeks and months to coincide with major spawning events [26,52]. By contrast, for most biomedical applications, NPs are designed to rapidly release a drug over a short time frame (i.e., burst release within minutes to hours) once they reach the target cell or location, which is facilitated by particle pore openings and/or *in situ* stimuli [44,53]. This feature is not beneficial to coral engineering applications.

Therefore, we engineered a fully inorganic, non-porous silica NP system combined with a hydrogel matrix to slow NP breakdown and control the diffusion of exometabolites, more closely

mimicking the natural reef microhabitat (Figure 4A) [54,55]. Silica NPs can be nonporous [56], solid [57], or porous via template functionalization [58]. For this application, we avoided mesoporous materials, because solvent diffusion into pores accelerates silica degradation. Instead, we selected silica capsules to enable a controlled, slow release of encapsulated molecules. The degradation of these NPs occurs through hydrolysis, which is influenced by saline environments. Increased ionic strength reduces electrostatic repulsion between silanol groups, promoting dissolution [45]. In addition, cations in the medium may form a protective shielding layer around the NPs, potentially enhancing their stability while modulating the release of silicate species, with pH variations further affecting the availability of reactive silanol groups [45].

To optimize the durability of SNAP-X, we engineered a hydrogel made from PEGDA and GelMA. PEGDA, a synthetic polymer, improves mechanical stiffness and crosslinking efficiency due to its uniform repeating units, which facilitate a high degree of polymerization and impart antifouling properties [55]. GelMA, a biopolymer, is incorporated for its excellent biocompatibility, biodegradability, and tunable mechanical properties [55]. The GelMA component in our hydrogel was highly porous due to its enrichment with OH groups [59], which have a high affinity for silica [60], and, therefore, offer protection from NP hydrolysis. This dual-component hydrogel approach was previously demonstrated to improve material performance by leveraging the complementary mechanical strength of PEGDA and the biological compatibility of GelMA [61], further supporting its application in SNAP-X.

Settlement experiments in both laboratory and mesocosm conditions with *M. capitata* demonstrated that SNAP-X coatings successfully induced metamorphosis and settlement onto target substrates, yielding up to a 20-fold increase compared with uncoated controls (Figures 5B and 6A). This represents a major improvement over previous approaches, which relied on chemical cues dissolved in ambient water [18,62] and often resulted in unattached metamorphosed larvae. The effectiveness of such chemical enrichment *in situ* is ultimately governed by the diffusive properties of the cues, which depend on both their molecular diffusion coefficients and the physical characteristics of the habitat [63,64]. Lighter compounds tend to dissipate more quickly, while heavier molecules accumulate at the substrate. On natural coral reefs, architectural features, such as crevices and cryptic habitats, create microenvironments with reduced flow and thickened diffusive boundary layers [8], allowing cues to accumulate and create concentration gradients. Similarly, in artificial reef designs, the incorporation of microarchitectural features, such as crevices (Figure 6B), will enhance the local concentration of exometabolites.

Given that SNAP-X is a photo-crosslinkable nanomaterial, it can be used with light-assisted 3D printing approaches [65,66] to create on-demand micropatterns tailored to optimize chemical signaling under different flow regimes. SNAP-X will be most effective when deployed in areas with reduced flow, such as the leeward side of flow-exposed structures (Figure S11 in the supplemental information online) or within microtopographies that increase larval retention time [8,67]. This interplay between biochemical signal retention and local hydrodynamics underscores the importance of designing artificial substrates that emulate the complex physicochemical microhabitats of natural reefs to maximize the likelihood of successful settlement. Future work will build on these findings to explore how the material impacts postsettlement growth and survivorship in extended studies.

Applications of SNAP-X for reef rehabilitation and hybrid reef engineering

Reef restoration endeavors have recently gained momentum through global pledges aimed at substantial recovery of natural ecosystem health and size (e.g., UN Decade for Ecosystem Restoration) [68]. Coral restoration typically uses either asexual fragmentation of adult corals or the production of sexually propagated juvenile corals [69,70]. Importantly, the latter offers the

advantage of greater genetic diversity [71] and, thus, is crucially needed to enhance long-term ecosystem resilience [72]. So far, enhancing sexually propagated corals *in situ* has been hampered by low settlement success on standard restoration substrates [73]. Here, we present a nature-inspired biomaterials approach using chemical landscape mimicry to augment recruitment microenvironments with potent settlement cues from CCA [18].

There is growing interest in identifying specific molecules that promote coral settlement, with promising candidates including tetrabromopyrrole (produced by biofilms [62,74]), cnidarian neurotransmitters [75], cycloprodigiosin [76], and morphogens derived from CCA [77]. While we successfully encapsulated a diverse range of settlement-inducing exometabolites [18], our nanoink platform is designed to be adaptable, allowing the potential incorporation of other cues to accommodate the potential needs of various coral species across different reef systems. This could involve modifications to the silica pore network [74] or hydrogel matrix [75], enabling the encapsulation of hydrophobic molecules, such as cycloprodigiosin [72] and CCA-derived morphogens [73]. This flexibility enables potential customization to match the ecological requirements of different coral species and environments. While no studies have directly tested whether exometabolites from Pacific CCA can induce settlement in Caribbean corals, it was demonstrated that CCA-derived exometabolites from morphologically similar CCA species also promote settlement in Caribbean corals [18]. The chemical classes of CCA exometabolite from this study (Pacific sea) are consistent with the exometabolites of CCA from the Caribbean sea and both studies primarily identified ion features classified as lipids, organic acids, and organic oxygen compounds as well as CCA-specific subnetworks (e.g., glycerophosphoethanolamine; Figure 2A,B [18]). This suggests that such metabolites influence coral settlement across regions, warranting further settlement assays with diverse coral species to explore this hypothesis. Rapid advances in cheminformatics [19] provide promising avenues for elucidating the diversity of chemical cues and biochemical mechanisms underpinning coral settlement. These developments will be critical for designing targeted, scalable interventions to support reef resilience and conservation [18].

Concluding remarks

In conclusion, we showed that biomimetic microhabitats can enhance coral settlement by over 20-fold (Figure 5A), highlighting their capacity to enhance coral recruitment and accelerate the formation of living hybrid reefs [78]. SNAP-X uses a modular, flexible ecosystem augmentation approach (Figure 1) and, therefore, can be integrated with existing artificial reef structures to enhance coral propagation (Figure 1C and Figure S10 in the supplemental information online). Strategic placement and distribution of SNAP-X-coated microhabitats on the reef infrastructure (Figure S10 in the supplemental information online) can be further used to optimize cue accumulation and, thus, settlement chances *in situ*. The core components of our biomimetic microhabitats are abundant and cheap to produce (e.g., silica and gelatin) [79,80] and free radical photopolymerization is among the fastest existing crosslinking methods [81], thus suggesting a viable pathway toward scalability (see Outstanding questions).

STAR★METHODS

Detailed methods are provided in the online version of this paper and include the following:

- KEY RESOURCES TABLE
- METHOD DETAILS
 - CCA exometabolites
 - Liquid chromatography tandem mass spectrometry (LC-MS/MS)
 - Metabolomic analytical pipeline
 - Nanoparticle formulation
 - Polymer synthesis

Outstanding questions

How can CCA exometabolites be produced at scale while preserving their bioactive properties?

Can SNAP-X be used to enhance settlement across a wider range of coral species and geographic regions?

What impact does SNAP-X have on the recruitment of other benthic organisms?

How does SNAP-X affect coral postsettlement health and growth?

How can SNAP-X be integrated with existing reef restoration frameworks for scalable deployment?

- Free radical photopolymerization of SNAP-X coating
- SNAP-X material characterization
- Cytochrome C release tests
- Coral settlement assays
- 3D chemical modeling of biomimetic microhabitats
- QUANTIFICATION AND STATISTICAL ANALYSIS

RESOURCE AVAILABILITY

Lead contact

Further information and requests for resources should be directed to, and will be fulfilled by, the lead contact, Daniel Wangpraseurt (dwangpraseurt@ucsd.edu).

Materials availability

Materials will be made available upon request from the lead contact, following standard Material Transfer Agreement (MTA) procedures.

Data and code availability

All data are available in the main text or the supplementary materials. Raw data have been deposited on Figshare (10.6084/m9.figshare.27915888).

R3D consortium

Ben Jones, Josh Levy, Sean Mahaffey, Aricia Argyris, Mark Aruda, Ian Robertson, Zhenhua Huang, Ayrton Medina-Rodriguez, Mert Gokdepe, Brady Halvorson, Jon Chase, Charlotte White, Cami Dillon, Kristian McDonald, Anna Mikkelsen, Josh Madin, Mollie Asbury, Jessica Haver, Hendrikje Jorissen, Nina Schiettekatte, Marion Chapeau, Rob Toonen, Chris Suchocki, Van Wishingrad, Christopher P. Jury, Dan Schar, Madeleine Hardt, Claire Lewis, Claire Bardin, Joshua Kualani, Crawford Drury, Kira Hughes, Josh Hancock, Carlo Caruso, Andrea Grottoli, Shannon Dixon, Ann Marie Hulver, Josh Voss, Allison Klein, Sid Verma, Alejandro Alvaro, Richard Argall, Kevin Chun, William Hicks, Alex LeBon, John Yeh, Aaron Thode, Oceane Boulais, Daniel Wangpraseurt, Samapti Kundu, Natalie Levy, Zahra Karimi, Stefan Kolle and Lindsey Badder

Author contributions

Conceptualization: S.K., D.W.; methodology: S.K., S.P., Z.A.Q., H.W., J.R.H., C.D., L.W.K., L.D.C., S.C., D.W.; investigation: S.K., S.P., Z.A.Q., H.W., J.C., T.N., N.L., Z.K., H.J., J.R.H., D.W.; visualization: S.K., Z.A.Q., H.W., J.C., D.W.; supervision: D.W., L.D.C., L.W.K.; writing – original draft: S.K., D.W.; writing – review and editing: all authors.

Acknowledgments

We acknowledge Vanessa De La Garza, Isabel Flores, Lindsey Badder, Ralph Torres, Neal Arakawa, Huixuan Kang, Claudia Tatiana Galindo Martínez, and Ricardo De-luna for help with experimental measurements. The authors acknowledge support from the UC San Diego Materials Research Science and Engineering Center (MRSEC). [Figure 1](#) was created using BioRender ([biorender.com](https://www.biorender.com)). Photo credits in [Figure 5A](#) belong to Christopher Wall (i), Mariana Rocha de Souza (ii), and Josh Hancock (iii). The research work presented in this article is supported by the Defense Advanced Research Projects Agency under the Reefense Program. Defense Advanced Research Projects Agency award HR001121S0012 (D.W. and C.D.), NSF award OCE-2118618 (L.W.K.), NSF award 1907434 (S.C.), GRFP award 2019252845 (Z.A.Q.), and NSF OCE-PRF 2308400 (Z.A. Q.) and by the Accelerating Innovation to Market Grant (D.W.) at UC San Diego as well as the CA CARES grant (D.W.) - a Climate Impact initiative by the University of California. The views, opinions and/or findings expressed are those of the author and should not be interpreted as representing the official views or policies of the Department of Defense or the US Government.

Declaration of interests

While no competing interests exist for any of the authors, the following information is provided for the sake of full transparency: D.W., S.K., S.C., and L.W.K. are authors on a provisional patent application related to this work. D.W. is founder of Hybrid Reef Solutions and is an advisory board member of the Coral Restoration Consortium, community practice for reef restoration. The authors declare that they have no other competing interests.

Supplemental information

Supplemental information to this article can be found online at <https://doi.org/10.1016/j.tibtech.2025.03.019>.

References

- Kusumoto, B. *et al.* (2020) Global distribution of coral diversity: biodiversity knowledge gradients related to spatial resolution. *Ecol. Res.* 35, 315–326
- Sing Wong, A. *et al.* (2022) An assessment of people living by coral reefs over space and time. *Glob. Chang. Biol.* 28, 7139–7153
- Eddy, T.D. *et al.* (2021) Global decline in capacity of coral reefs to provide ecosystem services. *One Earth* 4, 1278–1285
- Anthony, K.R.N. *et al.* (2020) Interventions to help coral reefs under global change—a complex decision challenge. *PLoS ONE* 15, e0236399
- Januchowski-Hartley, F.A. *et al.* (2020) Accreting coral reefs in a highly urbanized environment. *Coral Reefs* 39, 717–731
- Harrison, P.L. *et al.* (2021) Increased coral larval supply enhances recruitment for coral and fish habitat restoration. *Front. Mar. Sci.* 8, 750210
- Hadfield, M. and Paul, V. (2001) Natural chemical cues for settlement and metamorphosis of marine-invertebrate larvae. In *Marine Science* (McClintock, J.B. and Baker, B.J., eds), pp. 431–461, CRC Press
- Reidenbach, M.A. *et al.* (2009) Hydrodynamic forces on larvae affect their settlement on coral reefs in turbulent, wave-driven flow. *Limnol. Oceanogr.* 54, 318–330
- Speare, K.E. *et al.* (2023) Small-scale habitat selection by larvae of a reef-building coral. *Mar. Ecol. Prog. Ser.* 724, 67–79
- Harrington, L. *et al.* (2004) Recognition and selection of settlement substrata determine post-settlement survival in corals. *Ecology* 85, 3428–3437
- Whalan, S. *et al.* (2015) Larval settlement: the role of surface topography for sessile coral reef invertebrates. *PLoS ONE* 10, e0117675
- Ritson-Williams, R. *et al.* (2014) Larval settlement preferences of *Acropora palmata* and *Montastraea faveolata* in response to diverse red algae. *Coral Reefs* 33, 59–66
- Tebben, J. *et al.* (2014) A coralline algal-associated bacterium, *Pseudoalteromonas* strain J010, yields five new korormicins and a bromopyrrole. *Mar. Drugs* 12, 2802–2815
- Tebben, J. *et al.* (2015) Chemical mediation of coral larval settlement by crustose coralline algae. *Sci. Rep.* 5, 10803
- Tran, C. and Hadfield, M.G. (2011) Larvae of *Pocillopora damicornis* (Anthozoa) settle and metamorphose in response to surface-biofilm bacteria. *Mar. Ecol. Prog. Ser.* 433, 85–96
- Negri, A.P. *et al.* (2001) Metamorphosis of broadcast spawning corals in response to bacteria isolated from crustose algae. *Mar. Ecol. Prog. Ser.* 223, 121–131
- Kitamura, M. *et al.* (2007) Characterization of a natural inducer of coral larval metamorphosis. *J. Exp. Mar. Biol. Ecol.* 340, 96–102
- Quinlan, Z.A. *et al.* (2023) Coral larval settlement induction using tissue-associated and exuded coralline algae metabolites and the identification of putative chemical cues. *Proc. Biol. Sci.* 290, 20231476
- Wegley Kelly, L. *et al.* (2022) Distinguishing the molecular diversity, nutrient content, and energetic potential of exometabolomes produced by macroalgae and reef-building corals. *Proc. Natl. Acad. Sci. U. S. A.* 119, e2110283119
- Birrell, C.L. *et al.* (2008) Chemical effects of macroalgae on larval settlement of the broadcast spawning coral *Acropora millepora*. *Mar. Ecol. Prog. Ser.* 362, 129–137
- Gosselin, L.A. and Qian, P.Y. (1997) Juvenile mortality in benthic marine invertebrates. *Mar. Ecol. Prog. Ser.* 146, 265–282
- Penin, L. *et al.* (2010) Early post-settlement mortality and the structure of coral assemblages. *Mar. Ecol. Prog. Ser.* 408, 55–64
- Vardi, T. *et al.* (2021) Six priorities to advance the science and practice of coral reef restoration worldwide. *Restor. Ecol.* 29, e13498
- van Oppen, M.J.H. *et al.* (2015) Building coral reef resilience through assisted evolution. *Proc. Natl. Acad. Sci. U. S. A.* 112, 2307–2313
- Peixoto, R.S. *et al.* (2022) Harnessing the microbiome to prevent global biodiversity loss. *Nat. Microbiol.* 7, 1726–1735
- Roger, L.M. *et al.* (2023) Nanobioengineering for future coral reefs. *One Earth* 6, 778–789
- Roger, L. *et al.* (2023) Nanotechnology for coral reef conservation, restoration and rehabilitation. *Nat. Nanotechnol.* 18, 831–833
- Roger, L.M. *et al.* (2022) Engineered nanoceria alleviates thermally induced oxidative stress in free-living *Breviolum minutum* (Symbiodiniaceae, formerly Clade B). *Front. Mar. Sci.* 9, 960173
- Contardi, M. *et al.* (2023) Biodegradable Zein-based biocomposite films for underwater delivery of curcumin reduce thermal stress effects in corals. *ACS Appl. Mater. Interfaces* 15, 33916–33931
- Contardi, M. *et al.* (2021) Marine fouling characteristics of biocomposites in a coral reef ecosystem. *Adv. Sustain. Syst.* 5, 2100089
- Zych, A. *et al.* (2024) Underwater quick-hardening vegetable oil-based biodegradable putty for sustainable coral reef restoration and rehabilitation. *Adv. Sustain. Syst.* 8, 2400110
- LaVan, D.A. *et al.* (2003) Small-scale systems for in vivo drug delivery. *Nat. Biotechnol.* 21, 1184–1191
- Murphy, S.V. and Atala, A. (2014) 3D bioprinting of tissues and organs. *Nat. Biotechnol.* 32, 773–785
- You, S. *et al.* (2023) High cell density and high-resolution 3D bioprinting for fabricating vascularized tissues. *Sci. Adv.* 9, eade7923
- Wang, C. *et al.* (2022) Biohybrid materials: structure design and biomedical applications. *Mater. Today Bio* 16, 100352
- Darder, M. *et al.* (2007) Bionanocomposites: a new concept of ecological, bioinspired, and functional hybrid materials. *Adv. Mater.* 19, 1309–1319
- Ritson-Williams, R. *et al.* (2016) Patterns of larval settlement preferences and post-settlement survival for seven Caribbean corals. *Mar. Ecol. Prog. Ser.* 548, 127–138
- Jorissen, H. *et al.* (2021) Coral larval settlement preferences linked to crustose coralline algae with distinct chemical and microbial signatures. *Sci. Rep.* 11, 14610
- Abdul Wahab, M.A. *et al.* (2023) Hierarchical settlement behaviours of coral larvae to common coralline algae. *Sci. Rep.* 13, 5795
- Petras, D. *et al.* (2017) High-resolution liquid chromatography tandem mass spectrometry enables large scale molecular characterization of dissolved organic matter. *Front. Mar. Sci.* 4, 405
- Kunc, F. *et al.* (2019) Quantification of surface functional groups on silica nanoparticles: comparison of thermogravimetric analysis and quantitative NMR. *Analyst* 144, 5589–5599
- Saputra, O.A. *et al.* (2022) Organically surface engineered mesoporous silica nanoparticles control the release of quercetin by pH stimuli. *Sci. Rep.* 12, 20661
- Lin, Y.-S. and Haynes, C.L. (2010) Impacts of mesoporous silica nanoparticle size, pore ordering, and pore integrity on hemolytic activity. *J. Am. Chem. Soc.* 132, 4834–4842
- Prasetyanto, E.A. *et al.* (2016) Breakable hybrid organosilica nanocapsules for protein delivery. *Angew. Chem. Int. Ed Engl.* 55, 3323–3327
- Spitzmüller, L. *et al.* (2023) Dissolution control and stability improvement of silica nanoparticles in aqueous media. *J. Nanopart. Res.* 25, 40
- Zengin, A. *et al.* (2021) Injectable, self-healing mesoporous silica nanocomposite hydrogels with improved mechanical properties. *Nanoscale* 13, 1144–1154
- Andrade, D.B. *et al.* (2023) Hydrogel based on nanoclay and gelatin methacrylate polymeric matrix as a potential osteogenic application. *J. Funct. Biomater.* 14, 74
- Amaral, A.J.R. *et al.* (2018) Transiently malleable multi-healable hydrogel nanocomposites based on responsive boronic acid copolymers. *Polym. Chem.* 9, 525–537

49. Arno, M.C. *et al.* (2020) Exploiting the role of nanoparticle shape in enhancing hydrogel adhesive and mechanical properties. *Nat. Commun.* 11, 1420
50. Sun, Z. *et al.* (2024) Hydroxyethyl methacrylate corneal contact lenses doped with *N*-vinylpyrrolidone and silane-modified silica nanoparticles for enhanced UV absorption. *ACS Appl. Nano Mater.* 7, 705–714
51. Guo, Y. *et al.* (2020) Hydrogels and hydrogel-derived materials for energy and water sustainability. *Chem. Rev.* 120, 7642–7707
52. Padilla-Garniño, J.L. and Gates, R.D. (2012) Spawning dynamics in the Hawaiian reef-building coral *Montipora capitata*. *Mar. Ecol. Prog. Ser.* 449, 145–160
53. Singh, N. *et al.* (2011) Bioresponsive mesoporous silica nanoparticles for triggered drug release. *J. Am. Chem. Soc.* 133, 19582–19585
54. Giovannini, G. *et al.* (2017) Stabilizing silica nanoparticles in hydrogels: impact on storage and polydispersity. *RSC Adv.* 7, 19924–19933
55. Giovannini, G. *et al.* (2018) Improving colloidal stability of silica nanoparticles when stored in responsive gel: application and toxicity study. *Nanotoxicology* 12, 407–422
56. Tang, L. and Cheng, J. (2013) Nonporous silica nanoparticles for nanomedicine application. *Nano Today* 8, 290–312
57. Shirshahi, V. and Soltani, M. (2015) Solid silica nanoparticles: applications in molecular imaging. *Contrast Media Mol. Imaging* 10, 1–17
58. Zaharudin, N.S. *et al.* (2020) Functionalized mesoporous silica nanoparticles templated by pyridinium ionic liquid for hydrophilic and hydrophobic drug release application. *J. Saudi Chem. Soc.* 24, 289–302
59. Bupphathong, S. *et al.* (2022) Gelatin methacrylate hydrogel for tissue engineering applications—a review on material modifications. *Pharmaceuticals* 15, 171
60. Xue, L. *et al.* (2022) A composite hydrogel containing mesoporous silica nanoparticles loaded with *Artemisia argyi* extract for improving chronic wound healing. *Front. Bioeng. Biotechnol.* 10, 825339
61. Wang, Y. *et al.* (2018) Development of a photo-crosslinking, biodegradable GelMA/PEGDA hydrogel for guided bone regeneration materials. *Materials* 11, 1345
62. Sneed, J.M. *et al.* (2014) The chemical cue tetrabromopyrrole from a biofilm bacterium induces settlement of multiple Caribbean corals. *Proc. Biol. Sci.* 281, 20133086
63. Wangpraseurt, D. *et al.* (2012) In situ oxygen dynamics in coral-algal interactions. *PLoS ONE* 7, e31192
64. Steinberg, P.D. *et al.* (2001) Chemical mediation of surface colonization. In *Marine Chemical Ecology* (McClintock, J.B. and Baker, B.J., eds), pp. 367–400, CRC Press
65. Wangpraseurt, D. *et al.* (2020) Bionic 3D printed corals. *Nat. Commun.* 11, 1748
66. Wangpraseurt, D. *et al.* (2022) Bioprinted living coral microenvironments mimicking coral-algal symbiosis. *Adv. Funct. Mater.* 32, 2202273
67. Levenstein, M.A. *et al.* (2022) Millimeter-scale topography facilitates coral larval settlement in wave-driven oscillatory flow. *PLoS ONE* 17, e0274088
68. Waltham, N.J. *et al.* (2020) UN Decade on Ecosystem Restoration 2021–2030—what chance for success in restoring coastal ecosystems? *Front. Mar. Sci.* 7, 518980
69. Knowlton, N. *et al.* (2021) *Rebuilding Coral Reefs: A Decadal Grand Challenge*, International Coral Reef Society and Future Earth Coasts
70. Suggett, D.J. and van Oppen, M.J.H. (2022) Horizon scan of rapidly advancing coral restoration approaches for 21st century reef management. *Emerg. Top Life Sci.* 6, 125–136
71. Baums, I.B. *et al.* (2019) Considerations for maximizing the adaptive potential of restored coral populations in the western Atlantic. *Ecol. Appl.* 29, e01978
72. Quigley, K.M. *et al.* (2019) The active spread of adaptive variation for reef resilience. *Ecol. Evol.* 9, 11122–11135
73. Randall, C.J. *et al.* (2020) Sexual production of corals for reef restoration in the Anthropocene. *Mar. Ecol. Prog. Ser.* 635, 203–232
74. Sneed, J.M. *et al.* (2024) Coral settlement induction by tetrabromopyrrole is widespread among Caribbean corals and compound specific. *Front. Mar. Sci.* 10, 1298518
75. Erwin, P.M. and Szmant, A.M. (2010) Settlement induction of *Acropora palmata* planulae by a GLW-amide neuropeptide. *Coral Reefs* 29, 929–939
76. Petersen, L.-E. *et al.* (2021) Photosensitivity of the bacterial pigment cycloprodiginin enables settlement in coral larvae—light as an understudied environmental factor. *Front. Mar. Sci.* 8, 749070
77. Morse, D.E. *et al.* (1994) Morphogen-based chemical flypaper for *Agaricia humilis* coral larvae. *Biol. Bull.* 186, 172–181
78. van Oppen, M.J.H. *et al.* (2017) Shifting paradigms in restoration of the world's coral reefs. *Glob. Chang. Biol.* 23, 3437–3448
79. Mahony, O. *et al.* (2014) Silica-gelatin hybrids for tissue regeneration: inter-relationships between the process variables. *J. Sol-Gel Sci. Technol.* 69, 288–298
80. Smitha, S. *et al.* (2007) Synthesis of biocompatible hydrophobic silica-gelatin nano-hybrid by sol-gel process. *Colloids Surf. B Biointerfaces* 55, 38–43
81. Zennifer, A. *et al.* (2022) 3D bioprinting and photocrosslinking: emerging strategies & future perspectives. *Biomater. Adv.* 134, 112576
82. Weber Van Bosse, A. (1904) The Corallinaceae of the Siboga-expedition. *Siboga Expedition Monographs* 61, 1–110
83. Bosse, A.W. and Fosale, M.H. (1904) *The Corallinaceae of the Siboga-Expedition*, E.J. Brill
84. Dittmar, T. *et al.* (2008) A simple and efficient method for the solid-phase extraction of dissolved organic matter (SPE-DOM) from seawater. *Limnol. Oceanogr. Methods* 6, 230–235
85. Pluskal, T. *et al.* (2010) MZmine 2: modular framework for processing, visualizing, and analyzing mass spectrometry-based molecular profile data. *BMC Bioinformatics* 11, 395
86. Nothias, L.-F. *et al.* (2020) Feature-based molecular networking in the GNPS analysis environment. *Nat. Methods* 17, 905–908
87. Wang, M. *et al.* (2016) Sharing and community curation of mass spectrometry data with Global Natural Products Social Molecular Networking. *Nat. Biotechnol.* 34, 828–837
88. Shannon, P. *et al.* (2003) Cytoscape: a software environment for integrated models of biomolecular interaction networks. *Genome Res.* 13, 2498–2504
89. Dührkop, K. *et al.* (2019) SIRIUS 4: a rapid tool for turning tandem mass spectra into metabolite structure information. *Nat. Methods* 16, 299–302
90. Ludwig, M. *et al.* (2020) Database-independent molecular formula annotation using Gibbs sampling through ZODIAC. *Nat. Mach. Intell.* 2, 629–641
91. Koester, I. *et al.* (2022) Illuminating the dark metabolome of *Pseudo-nitzschia*-microbiome associations. *Environ. Microbiol.* 24, 5408–5424
92. Benjamini, Y. and Hochberg, Y. (1995) Controlling the false discovery rate: a practical and powerful approach to multiple testing. *J. R. Stat. Soc.* 57, 289–300
93. Jiang, S. *et al.* (2018) One-pot green synthesis of doxorubicin loaded-silica nanoparticles for in vivo cancer therapy. *Mater. Sci. Eng. C Mater. Biol. Appl.* 90, 257–263
94. Jaramillo, N. *et al.* (2018) Microemulsion assisted sol-gel method as approach to load a model anticancer drug inside silica nanoparticles for controlled release applications. *Colloid Interface Sci. Commun.* 24, 13–17
95. Auger, A. *et al.* (2011) A comparative study of non-covalent encapsulation methods for organic dyes into silica nanoparticles. *Nanoscale Res. Lett.* 6, 328
96. Yamauchi, H. *et al.* (1989) Surface characterization of ultramicro spherical particles of silica prepared by w/o microemulsion method. *Colloids Surfaces* 37, 71–80
97. Stetefeld, J. *et al.* (2016) Dynamic light scattering: a practical guide and applications in biomedical sciences. *Biophys. Rev.* 8, 409–427
98. Pecora, R. (1985) *Dynamic Light Scattering: Applications of Photon Correlation Spectroscopy*, Springer Science & Business Media
99. Chen, H. *et al.* (2005) Study on modification and dispersion of nano-silica. *J. Dispers. Sci. Technol.* 26, 27–37
100. López-Lorente, Á.I. and Mizakoff, B. (2016) Recent advances on the characterization of nanoparticles using infrared spectroscopy. *Trends Anal. Chem.* 84, 97–106

101. Almaghrabi, M. *et al.* (2023) Evaluating thermogravimetric analysis for the measurement of drug loading in mesoporous silica nanoparticles (MSNs). *Thermochim. Acta* 730, 179616
102. Loganathan, S. *et al.* (2017) Thermogravimetric analysis for characterization of nanomaterials. In *Thermal and Rheological Measurement Techniques for Nanomaterials Characterization* (Thomas, S. *et al.*, eds), pp. 67–108, Elsevier
103. Orlova, E.V. and Saibil, H.R. (2011) Structural analysis of macromolecular assemblies by electron microscopy. *Chem. Rev.* 111, 7710–7748
104. Seyedmahmoud, R. *et al.* (2019) Three-dimensional bioprinting of functional skeletal muscle tissue using GelatinMethacryloyl-alginate bioinks. *Micromachines* 10, 679
105. Gao, X. *et al.* (2009) Synthesis and characterization of functionalized rhodamine B-doped silica nanoparticles. *Opt. Mater.* 31, 1715–1719
106. Chen, Z. *et al.* (2013) Bioresponsive hyaluronic acid-capped mesoporous silica nanoparticles for targeted drug delivery. *Chemistry* 19, 1778–1783
107. Levenstein, M.A. *et al.* (2022) Composite substrates reveal inorganic material cues for coral larval settlement. *ACS Sustain. Chem. Eng.* 10, 3960–3971

STAR★METHODS

KEY RESOURCES TABLE

Reagent or resource	Source	Identifier
Chemicals		
0.2 μ m Polyethersulfone filter cartridges (Sterivex)	Millipore Sigma	Cat#SVGPL10RC
LC-MS grade hydrochloric acid (99.999% trace metals basis)	Millipore Sigma	Cat#339253
Bond Elut PPL SPE Cartridges	Agilent	Cat#12105004
LC/MS grade Water	Millipore Sigma	Cat#1.15333
LC/MS grade Methanol	Millipore Sigma	Cat#1.06035
Triton X-100	Millipore Sigma	Cat#X100
n-Hexanol	Millipore Sigma	Cat#8.04393
Cyclohexane	Millipore Sigma	Cat#179191
Tetraethyl Orthosilicate (TEOS)	Millipore Sigma	Cat#131903
30% Ammonium hydroxide solution	Millipore Sigma	Cat#221228
Ethanol	Millipore Sigma	Cat#459844
Gelatin from porcine skin	Millipore Sigma	Cat#G2500
Sodium carbonate	Millipore Sigma	Cat#223530
Sodium bicarbonate	Millipore Sigma	Cat#S6014
Methacrylic Anhydride	Millipore Sigma	Cat#276685
12–14kDa cutoff dialysis tubing	Spectrum Laboratories	Cat#08-700-150
Poly(ethylene) glycol diacrylate (PEGDA, Mn = 700 Da)	Millipore Sigma	Cat#455008
Lithium phenyl-2,4,6 trimethylbenzoylphosphinate (LAP)	TCI America™	Cat#L0290
Calcium carbonate (coral plugs)	Ocean Wonders	Cat#B00TNMYLZQ
Cytochrome C	Millipore Sigma	Cat#C2506
Deposited data		
Raw data	This paper	Figshare: 10.6084/m9.figshare.27915888
Software and algorithms		
COMSOL 5.6	COMSOL Multiphysics	https://www.comsol.com/product-download/5.6/windows
Origin Pro 2024	Origin, USA	https://www.originlab.com/demodownload.aspx
Biorender	Biorender	https://BioRender.com
Others		
405 nm LED source	Thorlabs, NJ, USA	https://www.thorlabs.com/thorproduct.cfm?partnumber=M405LP1-C1&gad_source=1&gclid=CjwKCAiAw5W-BhAhEiwApv4goleG2IsxflkxbswcratcbBzdAmFRmQ0mA_4VgnFYeasyjq5WK9hTIBoCyvUQAvD_BwE
Zetasizer ultra equipment with multi-angle dynamic light scattering (MADLS)	Malvern Panalytical, USA	https://www.malvernpanalytical.com/en/products
Fourier-transform infrared spectroscopy (FTIR)	Shimadzu IRAffinity-1	https://www.ssi.shimadzu.com/products/molecular-spectroscopy/ftir/index.html
Thermal analyzer	Netzsch model STA 449 F1 Jupiter	https://analyzing-testing.netzsch.com/en-US/products/special-offers/sta-449-f1-jupiter

(continued)

Reagent or resource	Source	Identifier
Transmission Electron Microscopy (TEM) Talos™ L120C TEM	ThermoFisher scientific	https://www.thermofisher.com/us/en/home/electron-microscopy/products/transmission-electron-microscopes/talos-l120c-tem.html
Rheometer	DHR30	https://www.tainstruments.com/hr-30/
Optical Coherence Tomography (OCT)	Thorlabs GmbH, Dachau, Germany	https://www.thorlabs.com/navigation.cfm?guide_id=2039
Plate reader	SpectraMax iD3	https://www.moleculardevices.com/products/microplate-readers/multi-mode-readers/spectramax-id3-id5-readers
Blue light excitation source	Sola Nightsea Light, USA	https://nightsea.com/products/sola-nightsea-light/
Digital microscope	Dino-Lite Premier digital microscope, USA	https://www.dinolite.us/?gad_source=1
Stereo microscope	Motic SMZ-168	https://www.microscope.com/motic-motic-smz-168-led-7-5x-50x-zoom-stereo-microscope.html

METHOD DETAILS

CCA exometabolites

CCA that was visually identified as *Hydrolython reinboldii* [82,83], was collected from Kaneohe Bay, Hawai'i. CCA was cleaned of epiphytes and maintained in flowthrough seawater outdoors at the Hawai'i Institute of Marine Biology. To extract settlement-inducing exometabolites, we incubated small pieces of CCA (covering a surface area 200-400 cm²) with 1 l of seawater for 12 hours during daytime [18]. Exometabolites were extracted from metabolite enriched seawater using a solid-phase extraction [19,84]. For this, seawater was filtered through 0.2 μm polyethersulfone filter cartridges (Sterivex, Millipore, UK) and acidified to pH 2 with LC-MS grade hydrochloric acid. The acidified filtrate was extracted on the solid-phase extraction (SPE) resin, Priority PolLutant (PPL, Agilent Bond Elut). PPL columns were cleaned and activated prior to extraction with LC-MS grade solvents [84]. To identify and remove any unwanted background molecular features (e.g., due to manual handling), blanks were collected using LC-MS grade water. PPL resins were dried with nitrogen gas and kept at -80°C for further use. SPE-bound metabolites were eluted in LC-MS grade methanol and the dried exometabolite powder was recovered by methanol evaporation using a rotary evaporator.

Liquid chromatography tandem mass spectrometry (LC-MS/MS)

SPE-bound metabolites were eluted in HPLC-grade methanol and injected into a Vanquish reverse-phase ultra-high-performance liquid chromatography system using C18 core-shell column (Kinetex C18, 150 × 2 mm, 1.8 μm particle size, 100 Å pore size, Phenomenex) electrospray ionization (ESI+) mass spectrometer (MS). An Orbitrap Elite Hybrid Linear Ion-Trap (Thermo Fisher Scientific) in data-dependent acquisition (DDA) of MS/MS spectra was performed to collect fragmentation spectra within a range of 150–1500 mass-to-charge ratio (*m/z*) in positive ion mode at a MS1 resolution of 120 000 and MS2 resolution of 17 500 [18]. LC-MS/MS was conducted at the Environmental and Complex Analysis Laboratory University of California, San Diego.

Metabolomic analytical pipeline

We characterized an 'ion feature' (also called molecular features) as an ion signal at specific retention times eluted off the UHPLC for which an MS/MS spectra is assigned. After conversion of the 26 raw MS-MS files to centroid mzXML, MzMine 3.9.0 [85] detected 268 unique ion features. Each ion feature was aligned to previously characterized spectral libraries using the Global Natural Products Social Molecular Networking (GNPS) platform [40,86,87]. Using the Feature based molecular network, GNPS additionally compared all ion features to cluster structurally similar ion features together into molecular subnetworks which were visualized in Cytoscape [88]. Using the *in silico* prediction tool CANOPUS, we predicted putative structures for each ion features [89,90]. A total of 12 experimental blanks were used to define background ion features (putative contaminants), described previously as ion features that had an average log₁₀ transformed extraction ion chromatogram (XIC) intensity across all samples less than 50% max abundance from experimental blanks [18,19,91]. This removal of background features, reduced the dataset to 76 ion features. Two-sided t-tests compared the exometabolites enriched in CCA pools to those observed in the seawater controls separately for each timepoint (FDR corrected t-test *p* < 0.05; [92]). Fifty-eight ion features were defined as significantly enriched in CCA

exometabolites (Text S1 in the supplemental information online). Data were \log_{10} transformed prior to any statistical analysis to approximate gaussian distribution.

Nanoparticle formulation

We evaluated several protocols for the one-pot synthesis and loading of non-porous silica nanoparticles with hydrophilic species, as previously developed for anticancer drugs [93,94], proteins [44], and dyes [95]. To synthesize inorganic non-porous silica nanoparticles, which encapsulate exometabolites and can be incorporated into a hydrogel matrix for slow release, we used a water-in-oil microemulsion sol-gel method [44,96]. This approach enables the direct entrapment of hydrophilic species within the forming silica framework. Triton X-100 (1.77 ml) and n-hexanol (1.8 ml) were dissolved in cyclohexane (7.5 ml). Separately, exometabolite dry powder extracted from one PPL cartridge was dissolved in 600 μ l of MilliQ water and added to 100 μ l of tetraethyl orthosilicate (TEOS) followed by vortexing for 5 min before this mixture was added to the organic solution. 50 μ l of 30% aqueous ammonia solution was added and the water-oil emulsion was stirred at 250 rpm overnight at a room temperature of 20°C. 20 ml of pure acetone was subsequently added in order to precipitate the exometabolite loaded silica nanoparticles. The material was recovered by centrifugation at 12 000 rpm, washed twice with ethanol, and three times with water. Finally, the nanoparticles were dried in a vacuum desiccator overnight. To explore varying loading amounts of exometabolites (0.1x, 0.5x, 1x, 5x, 10x), where 1x is equivalent to the dried metabolite powder extracted from 1 PPL cartridge [18], which is equivalent to 200-400 cm^2 of CCA surface area.

Polymer synthesis

Gelatin methacrylate (GelMA) was synthesized as described previously [65]. Briefly, porcine gelatin (Sigma Aldrich, USA) was mixed at 10% (w/v) 0.25 M carbonate-bicarbonate (CB) buffer (~pH 9.2-9.5) and stirred at 50°C until fully dissolved. Methacrylic anhydride (MA; Sigma Aldrich, USA) was added until a concentration of 8% (v/v) of MA was achieved. The reaction continued for 2 h at 50°C under constant stirring. The solution was then dialyzed against distilled water using 12–14 kDa cutoff dialysis tubing (Spectrum Laboratories, CA, USA) for 7 days at 40°C to remove any unreacted methacrylic groups from the solution. The GelMA was lyophilized at -80°C in a freeze dryer (Freezone, Labonco) for 1 week to remove the solvent. Poly(ethylene) glycol diacrylate (PEGDA, $M_n = 700$ Da) was purchased from Millipore-Sigma (St. Louis, MO). The photoinitiator lithium phenyl-2,4,6-trimethylbenzoylphosphinate (LAP) (TCI America™) was used to obtain the photopolymerizable prepolymer mixture by dissolving it in MilliQ water at 60°C via sonication to reach a stock solution of 4%.

Free radical photopolymerization of SNAP-X coating

The lyophilized GelMA was dissolved in MilliQ water to create a 15% w/v stock solution. Exometabolite loaded silica nanoparticles were uniformly dispersed in MilliQ water by vortexing for 1 min. SNAP-X was then created by mixing the GelMA stock solution, photoinitiator LAP, and PEGDA-700 at a final concentration of 5% w/v GelMA and 0.5% w/v LAP and 10% w/v PEGDA-700 and 6.25 w/v silica nanoparticles. The nanoink was then used to coat common coral restoration substrates made from calcium carbonate (coral plugs) via free radical photopolymerization [65]. For each plug, 120 μ l of the nanoink was used to coat the surface of the substrate, with 40 μ l applied to the base of the plug and 80 μ l applied to the top of the plug. Crosslinking was facilitated via rapid free radical photopolymerization induced using a 405 nm LED source (Thorlabs, New Jersey, USA) emitting 17 $\text{mW cm}^{-2} \text{ s}^{-1}$ for a total of 45 seconds exposure time. Hydrogel porosity was measured based on weight changes following ethanol immersion (Text S3 in the supplemental information online).

SNAP-X material characterization

We characterized the size of the nanoparticles using dynamic light scattering (DLS) and TEM imaging (Figure S2 in the supplemental information online) [97]. For DLS measurements, 10 mg of empty silica nanoparticles and exometabolite loaded silica nanoparticles were suspended in 1 ml FSW and incubated in the dark at 25°C shaking (80 rpm) condition. The samples in seawater were centrifuged and washed three times with dH_2O to avoid interferences due to seawater components (such as electrolytes). The DLS measurements were performed on dispersions of silica nanoparticles in dH_2O (pH 7) using a zetasizer ultra equipment with multi-angle dynamic light scattering (MADLS) technology (Malvern Panalytical, USA) and analyzed using a commercial software (ZS Xplorer, USA) [97,98].

To evaluate the successful loading of silica nanoparticles with exometabolites, we performed Fourier-transform infrared spectroscopy (FTIR) and thermogravimetric analysis (TGA). For the FTIR analysis, silica nanoparticles were obtained as fine powder after drying and the sample amount was chosen in order to completely cover the small transparent window of the ATR-FTIR chamber (~1 mg). The FTIR spectra were recorded using a high-resolution spectrometer (Shimadzu IRAffinity-1). The attenuated total reflectance spectra were

collected at a spectral resolution of 1 cm^{-1} with 45 scans from 600 to 4000 cm^{-1} [99,100] For TGA measurements, silica nanoparticles were heated from 25°C to 100°C at a speed of $2.6\text{ }^\circ\text{C min}^{-1}$, then heated from 100 to 800°C at a speed of $10^\circ\text{C min}^{-1}$, before being held at this temperature for a further 30 min. Measurements were carried out under a 20 ml min^{-1} airflow using a simultaneous thermal analyzer (Netzsch model STA 449 F1 Jupiter) [101,102].

Transmission electron microscopy (TEM) imaging was used to visually evaluate the shape and nanoarchitecture of the nanoparticles as well as their breakdown over three weeks following incubation with seawater. For TEM imaging, 10 mg of empty silica and exometabolites loaded silica nanoparticles were suspended in 1 ml FSW and incubated under shaking conditions (at 80 rpm) at 25°C in the dark for three weeks. Aliquots ($300\text{ }\mu\text{l}$) were taken weekly during the three-week experiment. Samples were centrifuged and washed three times with dH_2O to avoid interferences with seawater (due to e.g., the presence of salts). Diluted samples ($0.5\text{ mg nanoparticles / ml dH}_2\text{O}$, $5\text{--}10\text{ }\mu\text{l}$) were placed on TEM copper grids for 3-5 minutes.

The grids were first placed on a filter paper to remove any excess droplets. Afterwards, they were returned to the grid holder and left overnight in a well-ventilated place to ensure complete evaporation of the residual solvent. The samples were imaged with a Talos™ L120C TEM with a LaB6 electron source operating at a voltage of 120 kV with a beam current of $5\text{ }\mu\text{A}$ [103].

Rheological measurements were performed by using a DHR30 from TA Instruments to assess the mechanical behavior of the hydrogel and the nanoparticle loaded hydrogels. A 25 mm parallel plate was used with a Peltier plate to hold the temperature at 25°C . An isostrain of 1% and angular frequency range of $1\text{--}100\text{ rad/s}$ were used with a variable gap to correct for the swelling of the samples affecting the thickness [104]. Storage and loss modulus were plotted versus the angular frequency. The distribution of the nanoparticles within the hydrogel and the thickness of the hydrogel layer was measured through Optical Coherence Tomography (OCT) [65] (Thorlabs GmbH, Dachau, Germany).

Cytochrome C release tests

To investigate the release of chemical cues from the SNAP-X system, we used cytochrome C as a model molecule [44]. Cytochrome C was selected because its molecular weight (12 kDa) closely approximates the average molecular weight of exometabolites determined by LC/MS, suggesting a similar diffusion coefficient [18]. While CCA exometabolites comprise a complex mixture of compounds, many of which remain not fully characterized, cytochrome C was chosen for its hydrophilicity, making it a relevant proxy for the water-soluble fraction of exometabolites extracted from the cartridges. Although no single model molecule can fully replicate the release profile of this complex exometabolite mixture, cytochrome C provided a useful preliminary validation tool. Its strong absorption in the visible region enabled effective monitoring of release kinetics via UV/Vis absorption spectroscopy. It is important to note that the measured release kinetics reflect those of the model molecule, whereas individual exometabolites may diffuse at different rates depending on their specific properties.

To perform release kinetics studies with cytochrome C, nanoparticles were synthesized (as described above) using an initial loading concentration of cytochrome C of 1 mg/ml . To explore the benefits of stabilization through the hydrogel network, tests were conducted on both dispersed nanoparticles and the hybrid nanoparticle hydrogel system [105,106]. In the case of dispersed nanoparticles, 10 mg of nanoparticles were suspended in 1 ml of FSW and incubated under static and shaking conditions at 25°C in darkness. The nanoparticle suspension was centrifuged ($16\text{ }000\text{ rcf}$) every 24 h. The supernatant was discarded and the obtained nanoparticles were re-dispersed in 1 ml FSW [105]. A well plate reader (SpectraMax iD3) was used to quantify the peak absorbance of cytochrome C (410 nm) from the suspension [44]. The change in absorbance intensity was used to determine the percentage of cytochrome C released [44]. Likewise, for the hybrid nanoparticle hydrogel system, an equal amount of cytochrome C-loaded nanoparticles (10 mg per plug) were crosslinked within the hydrogel and on top of CaCO_3 plugs (see earlier). The coated plugs were incubated in six-well plates filled with 9 ml of FSW under the same condition as the dispersed particles. Aliquots ($300\text{ }\mu\text{l}$) were taken, replaced with an equal volume of FSW [106], and the release of cytochrome C was measured at specific time intervals. To account for any background absorption due to the hydrogel, we also performed measurements on hydrogels alone without nanoparticles.

Coral settlement assays

Montipora capitata larvae were reared following established best practices to three-four days post fertilization (Text S4 in the supplemental information online). Larval settlement was assessed in 6-well plates without water flow and in a flowthrough mesocosm

experiment. For 6-well plate experiments, the SNAP-X coating was tested for three different loading densities (0.1x, 1x, 10x concentration) and evaluated against uncoated control plugs and seawater controls ($n = 6$ plugs per treatment). Each plug was placed in a single well and filled with 7 ml of FSW. *M. capitata* larvae were first washed with FSW to remove debris and organic matter before 3 ml were added to each well (at a density of ~ 13 larvae ml^{-1}). Settlement assays were performed overnight in a 27°C incubator. To test the efficacy of SNAP-X under *in situ*-like conditions, we created a flowthrough mesocosm system that used natural seawater. Each treatment (SNAP-X 0.1, SNAP-X 1, SNAP-X 10, uncoated control) was replicated in three tanks, with six plugs per tank ($n = 18$ per treatment, Figure S8 in the supplemental information online). The volume of seawater in the tank was maintained at 0.5 l with an average outflow rate of ~ 3 ml s^{-1} . We added 100 ml of washed *M. capitata* larvae (at a density of 10 ml^{-1}) to each tank. After an incubation period of 12 hours, larval settlement was counted with the aid of a blue light excitation source (Sola Nightsea Light, USA) to improve larval/recruit visibility. We categorized larval behavior through visual observations and microscopy using a digital microscope (Dino-Lite Premier digital microscope, USA) coupled with a blue excitation source (Sola Nightsea Light, USA) and a stereo microscope (Motic SMZ-168) as settled (attached and metamorphosed) [18], dead/disintegrated, and swimming [62]. Larval settlement locations were also recorded as top, bottom and side of the CaCO_3 substrate [107].

3D chemical modeling of biomimetic microhabitats

Spatio-temporal models were built to simulate the 3D distribution of exometabolites released from SNAP-X coated substrates over 30 days. For this, we used the 'Reacting Flow, Diluted Species' feature of COMSOL Multiphysics v. 5.6 (<https://www.comsol.com>). To simulate the diffusion of a pool of exometabolites, we used a generalized diffusion coefficient ($1e^{-9}$ m^2/s) based on the diffusion of hydrocarbons in water. Exometabolites were released as a steady state flux based on measured cytochrome C release. The molecular release profile of the nanoparticle hydrogel system was modeled as a surface reaction producing exometabolites, located at the surface of the plug covered by the hydrogel in the experimental set-up. The reaction rate was obtained by fitting the kinetic release data of the nanoparticle hydrogel system loaded with cytochrome C after the initial swelling period (2-3 days). The mathematical description of the exometabolite release within a timeframe of 5 to 30 days is based on the nanoparticle dissolution behavior (Equation 1.) [45] and is used to model the combined processes resulting in cue release:

$$c = C_{max} (1 - e^{-at+b}) \quad [1]$$

$$dc/dt = C_{max} a e^{-at+b} \quad [2]$$

The 3D distribution of exometabolites released from a singular plug was then estimated at an incident flow velocity of 1 cm s^{-1} (Figure 5B,C in the main text). Simulations with multiple plugs attached to larger reef frameworks were also performed using higher ambient flow velocities (4 cm s^{-1} , Figure S10 in the supplemental information online).

QUANTIFICATION AND STATISTICAL ANALYSIS

All statistical analysis and data plotting was performed with Origin Pro 2024 (Origin, USA). Data were verified for normal distribution using Shapiro-Wilk tests with a significance level of $\alpha = 0.05$. Data were arcsine square root transformed if necessary. One-way analysis of variance (ANOVA) was used to assess statistical differences in coral settlement ($p < 0.05$) ($n = 6$). When statistical differences were observed, Tukey's HSD post-hoc comparisons were applied to determine which of the groups and experimental treatments were significantly different with a significance level of $\alpha = 0.05$.